1521-009X/51/4/499–508$35.00
DRUG METABOLISM AND DISPOSITION

dx.doi.org/10.1124/dmd.122.001129
Drug Metab Dispos 51:499–508, April 2023

Predictive Performance of Physiologically Based Pharmacokinetic Modelling of Beta-Lactam Antibiotic Concentrations in Adipose, Bone, and Muscle Tissues[S]

Pieter-Jan De Sutter, Pieter De Cock, Trevor N Johnson, Helen Musther, Elke Gasthuys, and An Vermeulen

Laboratory of Medical Biochemistry and Clinical Analysis, Department of Bioanalysis, Faculty of Pharmaceutical Sciences (P-J.DS., E.G., A.V.), Department of Basic and Applied Medical Science, Faculty of Medicine and Health Sciences (P.D-C), Ghent University, Ghent, Belgium; Department of Pharmacy and Department of Pediatric Intensive Care, Ghent University Hospital, Ghent, Belgium (P.D-C.); and Certara UK Limited, Sheffield, United Kingdom (T.N.J., H.M.)

Received October 6, 2022; accepted January 6, 2023

ABSTRACT

Physiologically based pharmacokinetic (PBPK) models consist of compartments representing different tissues. As most models are only verified based on plasma concentrations, it is unclear how reliable associated tissue profiles are. This study aimed to assess the accuracy of PBPK-predicted beta-lactam antibiotic concentrations in different tissues and assess the impact of using effect site concentrations for evaluation of target attainment. Adipose, bone, and muscle concentrations of five beta-lactams (piperacillin, cefazolin, cefuroxime, ceftazidime, and meropenem) in healthy adults were collected from literature and compared with PBPK predictions. Model performance was evaluated with average fold errors (AFEs) and absolute AFEs (AAFEs) between predicted and observed concentrations. In total, 26 studies were included, 14 of which reported total tissue concentrations and 12 unbound interstitial fluid (uISF) concentrations. Concurrent plasma concentrations, used as baseline verification of the models, were fairly accurate (AFE: 1.14, AAFE: 1.50). Predicted total tissue concentrations were less accurate (AFE: 0.68, AAFE: 1.89). A slight trend for underprediction was observed but none of the studies had AFE or AAFE values outside threefold. Similarly, predictions of microdialysis-derived uISF concentrations were less accurate than plasma concentration predictions (AFE: 1.52, AAFE: 2.32). uISF concentrations tended to be overpredicted and two studies had AFEs and AAFEs outside threefold. Pharmacodynamic simulations in our case showed only a limited impact of using uISF concentrations instead of unbound plasma concentrations on target attainment rates. The results of this study illustrate the limitations of current PBPK models to predict tissue concentrations and the associated need for more accurate models.

SIGNIFICANCE STATEMENT

Clinical inaccessibility of local effect site concentrations precipitates a need for predictive methods for the estimation of tissue concentrations. This is the first study in which the accuracy of PBPK-predicted tissue concentrations of beta-lactam antibiotics in humans were assessed. Predicted tissue concentrations were found to be less accurate than concurrent predicted plasma concentrations. When using PBPK models to predict tissue concentrations, this potential relative loss of accuracy should be acknowledged when clinical tissue concentrations are unavailable to verify predictions.

1. Introduction

Beta-lactam antibiotics are frequently used to prevent and treat infection of tissues by extracellular bacterial pathogens. Certain patient populations could benefit from pharmacokinetic (PK) optimization to improve treatment outcomes (Abdul-Aziz et al., 2020; Fratoni et al., 2021), and as with most drugs, this is conventionally done using plasma or serum concentration measurements instead of via local effect site concentrations. The use of plasma concentrations to drive pharmacodynamic (PD) relationships is often justified by the assumption that a rapid equilibrium between the unbound plasma concentrations and the unbound interstitial tissue concentrations is installed (free drug hypothesis) (Mariappan et al., 2013). In practice, the processes which govern the distribution of a drug from the vasculature to tissues are not instantaneous and are highly variable between patients. Therefore, it follows that the concentration in the target tissue can be a more relevant predictor of effect than the unbound plasma concentration (Eichler and Müller, 1998). Of course, the use of plasma concentrations in PK/PD modeling does not stem from a misunderstanding of these concepts, but rather from the issues associated with difficulties to sample tissue, as well as with quantification and interpretation of tissue drug concentrations (Lin, 2006). Taking a tissue biopsy, for example, is an invasive procedure only ethically feasible under certain circumstances (e.g., during surgery) and is not suitable for repeated sampling. Additionally, concentrations derived from whole tissue samples (homogenates) do not distinguish between intra- and extracellular concentrations (Mouton et al., 2008; Mariappan et al., 2013). Using microdialysis to probe unbound interstitial

This work received no external funding.
Johnson and Musther are employees of Certara UK Limited. All other authors declared no competing interests for this work.
dx.doi.org/10.1124/dmd.122.001129.
[S] This article has supplemental material available at dmd.aspetjournals.org.

ABBREVIATIONS: AAFE, absolute average fold error; AFE, average fold error; AUC, area under the curve; FE, fold error; Kp, tissue-to-plasma partition coefficient; MIC, minimal inhibitory concentration; PBPK, physiologically based pharmacokinetics; PD, pharmacodynamics; PK, pharmacokinetics; uISF, unbound interstitial fluid concentration.

(extracellular) tissue concentrations is a less invasive alternative to tissue biopsies, but involves a complicated and expensive procedure (Plock and Kloft, 2005).

In the absence of an efficient technique to measure effect site concentrations, the prediction of tissue concentrations becomes a useful tool. While not its main application, physiologically based pharmacokinetic (PBPK) modeling can offer an attractive alternative to achieve these goals, as tissue concentrations are explicitly modeled with a set of differential equations parameterized with physiologic data (e.g., tissue volume and composition) (Jones and Rowland-Yeo, 2013; El-Khateeb et al., 2021). Most PBPK tissue compartments rely on the assumption that the rate of tissue distribution is perfusion-limited (i.e., only restricted by the blood flow), in other words that capillaries of tissues are sufficiently discontinuous to allow diffusion to the extracellular space (Rowland and Tozer, 2011; Holt et al., 2019). This is not always the case. For example, diffusion through the blood-brain barrier is often limited by tight junctions and efflux transporters (Rowland and Tozer, 2011). Multi-compartmental permeability limited distribution models are required for such processes, which require in vitro permeability data to parameterize (Gaohua et al., 2016). The extent of distribution of a drug to specific tissues, quantified as tissue-to-plasma partition coefficients (Kps), is required as input for perfusion-limited PBPK models. Kp values can be obtained from in vivo rodent studies, but most commonly, they are predicted based on tissue composition and the physicochemical drug properties (Holt et al., 2019). These composition-based equations assume passive distribution and were validated based on observed Kp values in rodents and on volume of distribution at steady state observations in humans (Poulin and Theil, 2002; Rodgers and Rowland, 2007). While multiple studies have used these equations to predict concentrations in perfusion-limited tissues, only some of these predicted profiles have been verified with clinical observations (Garreau et al., 2022), mainly due to a lack of human tissue concentration data (Zhu et al., 2015, 2016, 2022; Guo et al., 2018; Alhadab and Brundage, 2020). Systematic verification of PBPK predictions in tissues has not been carried out, and therefore, little is known about their accuracy.

This study focuses on the accuracy and applicability of PBPK predicted tissues concentrations in humans. The primary aim was to compare clinically observed tissue concentrations with PBPK predictions for a selection of beta-lactam antibiotics (piperacillin, cefazoline, cefuroxime, ceftazidime, and meropenem) in perfusion-limited tissues (adipose, bone, and muscle). The secondary aim was to compare target attainment rates using either unbound plasma or unbound interstitial tissue concentrations in different virtual populations.

2. Materials and Methods

2.1. PBPK Models. PBPK predictions in plasma and tissues were performed for five beta-lactam antibiotics, namely piperacillin, cefazolin, cefuroxime, ceftazidime, and meropenem. The Simcyp Simulator V20 (Jamei et al., 2009) was used as the modeling platform. In this simulator, the distribution of drugs to perfusion-limited tissues is modeled using a well-stirred tank assumption (Jamei et al., 2014) (eq. 1):

$$\frac{dC_T}{dt} = \frac{Q_T}{V_T}\left(C_a - \frac{C_T}{(Kp/BP)}\right) \quad (1)$$

where C_T is the total tissue concentration, C_a is the total arterial blood concentration, Q_T and V_T represent the tissue blood flow and volume, respectively, BP is the blood-to-plasma concentration ratio, and Kp is the tissue-to-plasma partition coefficient. Unbound concentrations in the interstitial fluid were estimated based on the total tissue concentrations by multiplying the total tissue concentrations by the ratio of the free fraction in plasma to the Kp value (Equation 2, derivation in supplementary material):

$$\frac{dC_{ISF,u}}{dt} = \frac{fu_{plasma}}{Kp}\ \frac{dC_T}{dt} \quad (2)$$

where $C_{ISF,u}$ is the unbound concentration in the interstitial fluid and fu_{plasma} is the free fraction in plasma. This approach is based on two additional assumptions, namely: i) at distribution steady state, the unbound interstitial concentration equals the unbound plasma concentration (free drug hypothesis) and ii) an instant equilibrium between the interstitial and intracellular compartments of the tissue is installed.

For piperacillin, a compound model was developed while for the other drugs published models were used without any adaptation (Hsu et al., 2014; Zhou et al., 2016; Abduljalil et al., 2022). The specific drug-dependent input parameters are given in Table 1. The substrates are low molecular weight ($\leq$ 547 g/ml) hydrophilic acids (LogP $\leq$ 0.50) and are not expected to enter red blood cells (blood-to-plasma ratio = 0.55). The substrates mainly differ in the extent to which they are bound to serum albumin (2%, meropenem – 77%, cefazolin). Tissue-to-plasma partition coefficients (Kp) were estimated based on the Rodgers & Rowland equations (Rodgers and Rowland, 2007). For cefazolin and cefuroxime, the models apply a scalar of 0.7 to the Kp predictions to better fit the plasma concentrations in the original model development studies (Hsu et al., 2014; Abduljalil et al., 2022). The piperacillin model was verified for plasma predictions with published data in healthy volunteers receiving single and multiple doses (3 g, 4 g, and 6 g) of piperacillin (-tazobactam). As no changes were made to the input parameters of the other substrate models, they were deemed fit for purpose based on the verifications carried out by the original model authors (Hsu et al., 2014; Zhou et al., 2016; Abduljalil et al., 2022).

The sensitivity of the models to changes in Kp values was evaluated by simulating single-dose (1 g bolus) regimens of the five antibiotics when Kp values were predicted with the following alternative methods: Poulin and Theil with a Berezhkovskiy correction (Poulin and Theil, 2002; Berezhkovskiy, 2004) (Method 1 in Simcyp), Rodgers and Rowland with ion membrane permeability (Method 3 in Simcyp), and the Schmitt method (Schmitt, 2008). The last method is not available in Simcyp V20 and was therefore implemented using the R script and uniform tissue distribution proposed by Utsey and colleagues (Utsey et al., 2020). The resulting alternative Kp values are given in Supplemental Table 1, together with the original Kp values predicted with the Rodgers and Rowland method ((Rodgers and Rowland, 2007), Method 2 in Simcyp).

2.2. Collection of Observed Data. Studies which reported concentrations of the selected beta-lactam antibiotics in non-pathologic perfusion-limited tissues of adult humans were identified through a structured PubMed search. Non-pathologic tissue was defined as not infected and not originating from hypothermic or obese subjects. The perfusion-limited tissues evaluated included adipose (fatty tissue), bone, and muscle (skeletal or cardiac muscle). When multiple studies for a given tissue-drug pair were available, the most comprehensive and representative study was selected based on the following ordered criteria: i) plasma data available, ii) relatively healthy population, iii) study not yet included in the work, iv) most recent suitable study. This last criterion (publication year) was chosen as a reproduceable selection criterion over harder to define metrics, such as richness of sampling or data quality. The study search procedure was done for total- (biopsy homogenate) and unbound interstitial fluid (uISF, obtained by microdialysis) tissue concentrations separately.

For each of the studies, the following parameters were collected to inform the design of the simulations: number of subjects, minimum and maximum age, number of female subjects, and the dosing regimen administered. Other physiologic data needed for the simulations were sampled from a reference patient population ("*North European Caucasian*" in the simulator). The following PK profiles and parameters were collected for model verification: concentration-time profiles in tissue and plasma, area under the curve in plasma (AUC_{plasma}), AUC in tissue (AUC_{tissue}) and penetration ratio ($AUC_{tissue}/AUC_{plasma}$). Data from plots were digitized with the aid of WebPlotDigitizer (Rohatgi, 2021). When tissue concentrations were expressed as a mass/mass ratio they were converted to mass/volume concentrations by multiplying them with the tissue densities used in the simulator: 0.923 kg/L for adipose, 1.85 kg/L for bone, and 1.04 kg/L for muscle, respectively.

2.3. PBPK Model Verification. For model verification, PBPK predicted concentration-time profiles and PK parameters in plasma and tissue were compared with observed data. This was done by calculating fold errors (FE) for each observed concentration or parameter with eq. 3:

$$FE = \frac{X_{Predicted}}{X_{Observed}} \quad (3)$$

TABLE 1

Input parameters of the PBPK compound models

Drug	Piperacillin	Cefazolin	Cefuroxime	Ceftazidime	Meropenem
Beta-lactam class	Penicillin	Cephalosporin	Cephalosporin	Cephalosporin	Carbapenem
Physicochemistry & blood binding					
Molecular weight (g/mol)	517.6 [1]	454.5	424.4	546.6	383.5
Compound type	Monoprotic acid	Monoprotic acid	Monoprotic acid	Diprotic acid	Monoprotic acid
Dissociation constants (pKa)	4.41 [2]	3.60	3.15	2.77 & 3.88	3.47
Octanol-to-water partition coefficient ($LogP_{o:w}$)	0.50 [3]	−0.58	−0.90	−4.55	−4.35
Blood-to-plasma ratio (B/P)	0.55 [4]	0.55	0.55	0.55	0.55
Free fraction in plasma (f_u)	0.80 [5]	0.225	0.67	0.90	0.98
Main serum binding protein	Albumin [6]	Albumin	Albumin	Albumin	Albumin
Distribution model (full PBPK)					
V_{ss} prediction method	Rodgers & Rowland	Rodgers & Rowland	Rodgers & Rowland	Rodgers & Rowland	Rodgers & Rowland
Global tissue-to-plasma (Kp) Scalar	1.0	0.7	0.7	1.0	1.0
Elimination					
Renal clearance	GFR + transport	GFR + transport	GFR + transport	CL_R typical = 6.8 L/h	CL_R typical = 8.4 L/h
CL_{int} OAT1 (μL/min/10^6 cells) {RAF/REF}		0.208 {1.0}	9.62 {1.0}		
CL_{int} OAT3 (μL/min/10^6 cells) {RAF/REF}	0.4875 {11.6}[a] [5]	7.28 {1.0}			
CL_{int} MRP4 (μL/min/10^6 cells) {RAF/REF}		41.43 {1.0}	10.00 {1.0}		
Additional systemic clearance	4.4 L/h [7]	CL_{int} HLM = 0.436 μL/min/mg protein		0.1 L/h	3.6 L/h
Validation reference	Supplemental Material (Supplemental Figure 1 & Supplemental Table 2)	(Abduljalil et al., 2022)	(Hsu et al., 2014)	(Zhou et al., 2016)	(Zhou et al., 2016)

[a]Lumped CL_{int} for OAT1 & 3.

[1-7]: references: 1: Pubchem, 2: (Sörgel and Kinzig, 1993), 3: (Benet et al., 2011), 4: (Cristea et al., 2021), 5: (Wen et al., 2018), 6: (Fisher et al., 2019), 7: (Bulitta et al., 2010).

CL_{int}, in vitro intrinsic clearance; CL_R typical, typical renal clearance for a healthy 20-30 year old healthy male; GFR, glomerular filtration rate; HLM, human liver microsomes; MRP4, multidrug resistance-associated protein (apical efflux transporter); OAT1-3, organic anion transporter 1-3 (basal uptake transporters); RAF/REF, Relative Activity Factor or Relative Expression Factor; V_{ss}, volume of distribution at steady state.

where X is a PK parameter of interest or a concentration at a specific timepoint. The average fold error (AFE) and the absolute average fold error (AAFE) for all concentrations of a study were calculated with eqs. 4 and 5, respectively:

$$AFE = 10^{\frac{1}{n}\sum log(FE)} \quad (4)$$

$$AAFE = 10^{\frac{1}{n}\sum |log(FE)|} \quad (5)$$

where n is the number of observations and FE the fold error calculated by eq. 3. Simulations were deemed successful when FEs of PK parameters were within twofold (0.5–2) and when the AFE and AAFE of the concentration-time profile were within twofold and smaller or equal to 2, respectively. The overall AFE and AAFE were calculated by putting the study specific AFE or AAFE into eqs. 4 and 5, respectively.

2.4. PBPK-PD Simulations. To evaluate the impact of using effect site concentrations instead of plasma concentrations on PK/PD target attainment in different populations, standard and high dosage regimens recommended by the European Committee on Antibiotic Susceptibility Testing (The European Committee on Antimicrobial Susceptibility Testing, 2022) were simulated. For the first dose of each of the regimens, the time during which the concentration exceeded the non-species-specific resistant minimal inhibitory concentration breakpoint (MIC) was calculated as a percentage of the dosage interval (fT>MIC). Investigated concentrations were unbound plasma and uISF adipose concentrations. Adipose was chosen as the example tissue as its perfusion changes in obese patients, a population evaluated in the simulations. Targets for fT>MIC were set at 50% for piperacillin, 60% for the cephalosporins and 40% for meropenem (Masich et al., 2018). Simulations were done with 1000 virtual patients (49.8% male, between 20 and 80 years old) sampled from a reference population (*North European Caucasian*), a population with a cardiac output twice that of the reference population, a population with a cardiac output half of the reference population, an obese (body mass index (BMI) from 30–40) population, and a morbidly obese (BMI > 40) population. The obese populations were developed by Ghobadi et al. and differ from the reference population in terms of body weight, renal function, cardiac output, and plasma protein concentrations (Ghobadi et al., 2011).

3. Results

3.1. Piperacillin PBPK Model Development and Verification. First, a PBPK model of piperacillin was developed and verified using plasma concentrations in healthy volunteers. PBPK predictions for piperacillin in plasma after single and multiple intravenous administration are shown in the supplementary materials (Supplemental Fig. 1). Of the eight simulated studies, seven passed the model performance criteria (Supplemental Table 2). The overall AFE and AAFE for the plasma concentrations were 0.85 and 1.44, respectively. The overall AFE and AAFE of the six reported AUC values were 0.84 and 1.19, respectively. The only study which did not meet the verification criteria had an AFE and an AAFE for the plasma profiles of 0.48 and 2.10 and an FE for the AUC of 0.45, indicating that the PBPK model marginally underpredicted the observed concentrations. However, as no general trend for underprediction could be discerned across the seven studies which passed the model performance criteria (overall AFE = 0.95 and 0.94 for profiles and AUC respectively), the piperacillin PBPK model was deemed fit for purpose.

3.2. PBPK Model Verifications of Tissue and Concurrent Plasma Concentrations. The PubMed search to identify studies reporting tissue concentrations of the five beta-lactams yielded 78 studies which fitted the inclusion criteria, 26 of which were selected for model verification (Supplemental Table 3). Study subjects were mainly non-obese patients without reported renal insufficiency undergoing elective surgical procedures (Supplemental Table 4). All 26 included studies except one (Kaukonen et al., 1995) reported plasma concentrations.

Study-specific simulation inputs and model verification assessments are given in Table 2. Details regarding the applied analytical procedures are summarized in Supplemental Table 5.

3.2.1. Accuracy of concurrent plasma concentrations. The observed and predicted plasma concentration-time profiles of the five beta-lactams are presented in Figs. 1 and 2. In general, observed plasma concentrations were captured well by the PBPK simulations as all but three studies (79%) complied with the beforementioned model performance criteria (Table 2). The overall AFE and AAFE were 1.14 and 1.50, respectively (Fig. 3A), indicating a minor trend for overprediction (+14%). Of the three studies which did not pass the model performance criteria (AFE and AAFE within twofold), one was noticeably overpredicted by the model, having an AFE and AAFE larger than 3 (Brunner et al., 2000). While piperacillin was administered in two of the three inaccurately predicted studies, no statistically significant differences in AAFEs between drugs could be discerned (Kruskal-Wallis, $P = 0.2$). Ten studies reported plasma AUC values, eight of which were within 2-fold of the predictions (fold errors in Table 2, AUC values in Supplemental Table 6).

3.2.2. Accuracy of total tissue homogenate concentrations. Of the 26 included studies, fourteen reported total tissue homogenate concentrations. These biopsy concentrations spanned all drug-tissue pairs except for meropenem in adipose tissue, for which no suitable study could be identified. The observed and PBPK predicted total tissue concentrations are given in Fig. 1. Half of the simulated concentration-time profiles in tissue (7/14) did not pass the model performance criteria (AFE and AAFE within twofold). All AFEs and AAFEs were, however, within a more lenient 3-fold interval (Table 2). The overall AFE and AAFE were 0.68 and 1.89, respectively, indicating that the models in general underpredicted the observed total tissue concentrations (-32%) (Fig. 3B). The time interval when tissue samples were collected was limited, with most observations being between 0.5 and 2 hours postdose and no noticeable trend of AFE in function of time could be picked up (Supplemental Fig. 2). None of the studies reported AUC_{tissue} and this parameter was therefore not compared with simulated data.

3.2.3. Accuracy of unbound interstitial fluid concentrations. Twelve studies were included which reported microdialysis (uISF) concentrations of the selected drugs (Table 2). No suitable studies could be identified which probed ceftazidime concentration in the interstitial space and not all remaining tissue-drug pairs could be assessed due to a lack of studies reporting on muscle and bone uISF concentrations. The observed and PBPK predicted uISF tissue concentrations are given in Fig. 2. Half of the simulated concentration-time profiles in uISF of tissue (6/12) did not pass the model performance criteria (AFE and AAFE within 2-fold) (Table 2). Two of those studies had AFE and AAFE outside the 3-fold criteria (Brunner et al., 2000; Schwameis et al., 2017). The overall AFE and AAFE were 1.52 and 2.32, respectively, indicating that the models were mostly inaccurate and tended to overpredict the observed uISF concentration profiles (+52%) (Fig. 3C). Additionally, a small trend for larger AFE at earlier sample points could be discerned (Supplemental Fig. 2). Of the nine observed AUC_{tissue} parameters, five were within 2-fold of the predicted value (fold errors in Table 2, AUC values in Supplemental Table 6). Eleven studies reported $AUC_{tissue}/AUC_{plasma}$ ratios, of which eight were within 2-fold of the predicted values (fold errors in Table 2, AUC values in Supplemental Table 6).

3.3. Sensitivity of the Models to Alternative Kp Values. The sensitivity of the predicted Kp values to different estimation methods is given in Supplemental Table 1. Bone and muscle Kp values are generally more than 2-fold higher when the Berezhkovskiy-corrected Poulin and Theil method or Schmitt method is applied instead of the Rodgers and Rowland equations. These increases are most pronounced for muscle and for the corrected Poulin and Theil method. For adipose tissue, the predicted Kp values are more consistent across the different methods. When the Rodgers and Rowland method is extended to model ion permeability, Kp values are consistently lower across antibiotics and tissues, although the decreases are minor (maximum -29%). The variability in Kp values also translates to differences in simulated concentration--time profiles (Supplemental Fig. 3). With the corrected Poulin and Theil and Schmitt methods, tissue concentrations are consistently higher than with the original models (Rodgers and Rowland method), especially for bone and muscle. Furthermore, changing the Kp estimation method also noticeably changes the plasma concentration profiles.

3.4. PBPK-PD Simulations in Virtual Populations. The PBPK simulated concentration profiles of the five beta-lactams in the different virtual populations are given in Supplemental Fig. 4 (standard dosage) and Supplemental Fig. 5 (high dosage). Relevant physiologic summary characteristics of the populations are presented in Supplemental Table 7. In Fig. 4 and Supplemental Fig. 6, the PK/PD target attainment (using *f*T>MIC) of respectively standard and high dosage regimens was calculated based on unbound plasma and uISF adipose tissue concentration profiles and conventional PK/PD target values.

The mean PK/PD target attainment rate (*f* T>MIC) for the standard dosage based on unbound plasma concentrations exceeded the conventional targets in the reference population for all beta-lactams except cefuroxime (Fig. 4). When the uISF adipose concentration was used to drive the PK/PD simulations, the same conclusions could be drawn, with slight increases in time above MIC (increase of 2–5% *f*T>MIC). Increasing the cardiac output of the reference population by a 2-fold (i.e., high cardiac output population) yielded similar *f* T>MIC as in the reference scenario, with the exception that the difference in target attainment between unbound plasma and uISF of adipose tissue became smaller (increase of 1–2% *f* T>MIC when using uISF concentrations). Decreasing the cardiac output of the reference population by 50% (i.e., low cardiac output population) resulted in similar target attainment with slightly increased differences between unbound plasma and uISF of adipose tissue target attainment (increase of 5–12% *f* T>MIC when using uISF concentrations) (Supplemental Fig. 7). Simulating the standard dosage regimens in an obese population (BMI 30–40) resulted in lower PK/PD target attainment with mean times above the MIC being below target for cefuroxime, ceftazidime and meropenem. Simulations with a morbidly obese population (BMI > 40) further lowered target attainment with piperacillin being the only beta-lactam reaching an adequate time above the MIC for standard dosages. For both obese populations relative differences in target attainment when using unbound plasma or uISF adipose concentrations were similar as in the reference population (increase of 1–4% *f* T>MIC when using uISF concentrations).

When high dosage regimens were simulated (Supplemental Fig. 5), PK/PD target attainment increased to the extent that for all drugs except cefuroxime, all virtual populations had *f* T>MIC above the conventional targets (Supplemental Fig. 6). Relative differences between PK/PD target attainment when using unbound plasma or uISF adipose concentrations were similar to what was observed with the standard dosages.

As species-specific breakpoints can deviate from the non-species specific breakpoint (Supplemental Table 8), the effect of varying the MIC on target attainment was also evaluated. The relative differences in target attainment between unbound plasma and uISF remain fairly constant when the MIC target is altered (Supplemental Fig. 8 for standard dosage, Supplemental Fig. 9 for high dosage). Only when the MIC breakpoint is high and associated target attainment low does the *f* T>MIC based on uISF become slightly smaller than target attainment based on unbound plasma concentrations.

TABLE 2

Accuracy of model predictions in tissue and plasma

Drug-matrix pair	Simulation parameters				Physiologically based pharmacokinetic (PBPK) model assessment							Reference observed data
					Plasma Profiles		Tissue Profiles		FE area under the curve (AUC)			
	IV dose (infusion duration)	N	Age in years (min-max)	Females	AFE	AAFE	AFE	AAFE	Plasma	Tissue	Tissue/Plasma	
Piperacillin												
Adipose (total)	4 g (30min)	18	29–77	50%	0.88	1.42	1.48	1.48	0.88	N.R.	N.R.	(Kinzig et al., 1992)
Bone (total)	3 g (30min)	9	44–86	30%	0.84	1.31	0.50	2.05	N.R.	N.R.	N.R.	(Incavo et al., 1994)
Skeletal muscle (total)	5 g (30min)	14	21–74	50%[a]	0.68	1.71	0.91	2.06	N.R.	N.R.	N.R.	(Russo et al., 1982)
Adipose (uISF)	4 g (30min)	15	18–65[a]	60%	1.20	1.60	1.29	1.89	N.R.	N.R.	N.R.	(Busse et al., 2021b)
Adipose (uISF)	4 g (10min)	6	25–37	0%	3.29	3.29	9.33	9.33	3.10	7.32	2.25	(Brunner et al., 2000)
Skeletal muscle (uISF)	4 g (10min)	6	60–72	17%	0.48	2.07	0.92	1.28	0.47	0.88	1.78	(Joukhadar et al., 2001)
Cefazolin												
Adipose (total)	1 g (4min)	10	52–79	20%	1.54	1.54	0.50	2.00	N.R.	N.R.	N.R.	(Ohge et al., 1999)
Bone (total)	2 g (15 min)	43	59–91	84%	1.26	1.32	0.50	2.12	N.R.	N.R.	N.R.	(Yamada et al., 2011)
Skeletal muscle (total)	2 g (25 min)	11	18–65[a]	50%	1.30	1.43	0.49	2.03	N.R.	N.R.	N.R.	(Sinagowitz et al., 1976)
Adipose (uISF)	2 g (1min)	7	42–61	46%	1.34	1.34	1.28	1.28	N.R.	N.R.	0.96	(Brill et al., 2014)
Adipose (uISF)	1 g (5min)	30	19–65	17%	1.46	1.46	1.87	1.87	1.12	1.58	1.35	(Roberts et al., 2015)
Adipose (uISF)	2 g (3 min)	12	59–81	0%	1.04	1.29	1.43	1.65	1.71	2.01	1.17	(Douglas et al., 2011)
Cefuroxime												
Adipose (total)	1.5 g (2min)	12	27–66	67%	1.09	1.10	0.35	2.86	N.R.	N.R.	N.R.	(Huizinga et al., 1989)
Bone (total)	1.5 g (10min)	40	47–83	38%	0.99	1.59	0.71	1.77	N.R.	N.R.	N.R.	(Gergs et al., 2020)
Skeletal muscle (total)	3 g (15min)	25	59–95	96%	N.R.	N.R.	0.82	1.23	N.R.	N.R.	N.R.	(Kaukonen et al., 1995)
Adipose (uISF)	1.5 g (10 min)	10	45–67	70%	1.17	1.27	0.83	1.87	1.23	0.80	0.61	(Hanberg et al., 2021)
Bone (uISF)	1.5 g (15 min)	9	58–76	0%	1.25	1.49	0.97	2.68	1.14	1.09	0.97	(Tøttrup et al., 2019)
Skeletal muscle (uISF)	1.5 g (10 min)	10	45–67	70%	0.87	1.23	0.36	3.08	0.98	0.56	0.56	(Schwameis et al., 2017)
Ceftazidime												
Adipose (total)	2 g (5min)	7	18–65[a]	50%[a]	1.64	1.64	1.05	1.57	N.R.	N.R.	N.R.	(Loebis, 1985)
Bone (total)	2 g (1min[a])	14	38–79	50%[a]	1.03	1.18	0.46	2.18	N.R.	N.R.	N.R.	(Wittmann et al., 1981)
Skeletal muscle (total)	2 g (5min)	9	18–65[a]	50%[a]	1.20	1.20	0.40	2.52	N.R.	N.R.	N.R.	(Loebis, 1985)
Meropenem												
Bone (total)	0.5 g (30 min)	15	29–75	47%	2.43	2.43	1.27	1.80	N.R.	N.R.	N.R.	(Sano et al., 1993)
Cardiac muscle (total)	1 g (7.5min)	25	47–75	72%	0.71	1.58	1.16	1.44	N.R.	N.R.	N.R.	(Newsom et al., 1995)
Adipose (uISF)	1 g (30 min)	15	31–64	87%	1.02	1.39	2.32	2.63	N.R.	N.R.	3.23	(Busse et al., 2021c)
Adipose (uISF)	1 g (30min)	15	30–70	13%	1.36	1.46	2.88	2.88	1.07	2.12	2.04	(Simon et al., 2020)
Skeletal muscle (uISF)	1 g (20 min)[b]	7	30–75	0%	0.88	1.26	2.09	2.27	1.08	2.29	1.63	(Tomaselli et al., 2004)

[a]Parameter not disclosed in study report.
[b]Fifth dose of a 8-hourly regimen.
AAFE, absolute average fold error; AFE, average fold error; FE, fold error; IV, intravenous; N, number of study subjects, simulations were done with N*10 virtual subjects; N.R., not reported; uISF, unbound concentration in interstitial fluid.

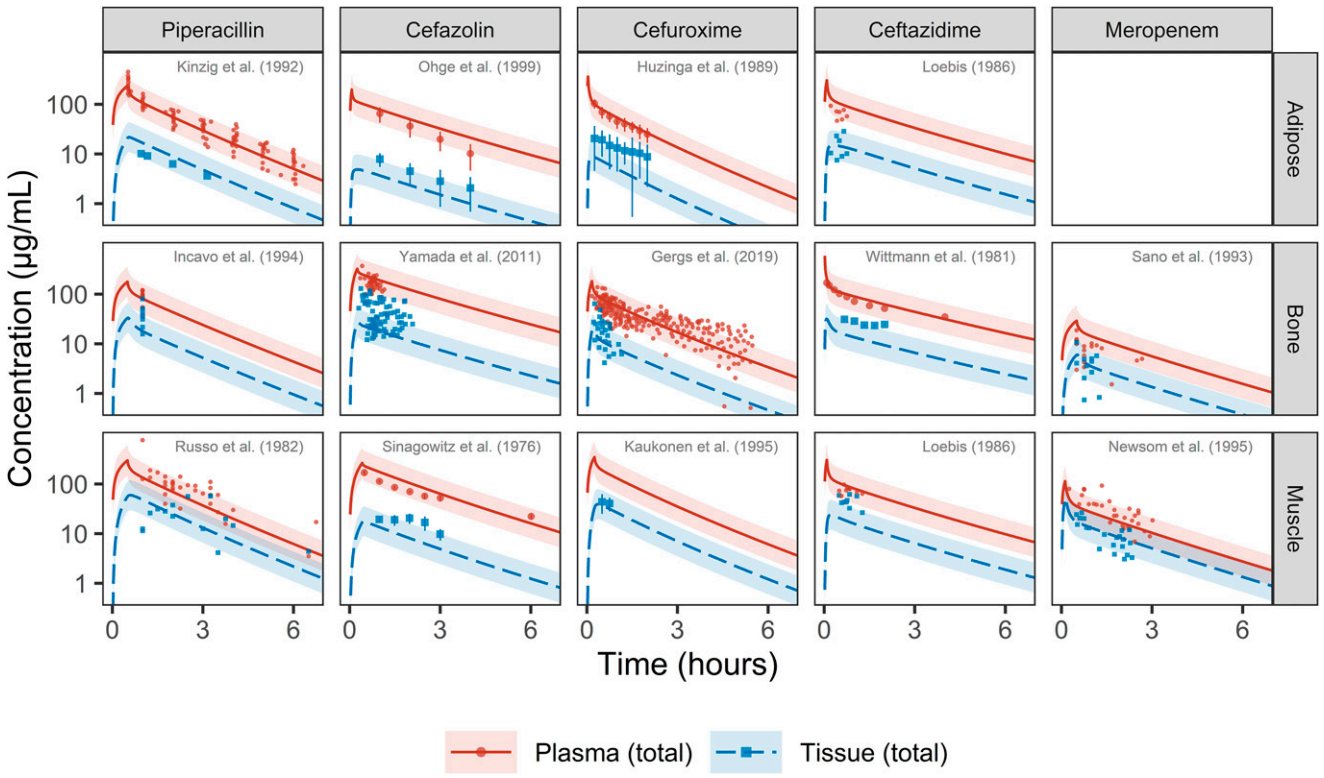

Fig. 1. PBPK-predicted (lines) and observed (squares and circles) concentrations of five beta-lactam antibiotics in plasma (red continuous lines and circles) and three different tissues (blue dashed lines and squares). Tissue concentrations are total concentrations of tissue biopsy homogenates, and plasma concentrations are total concentrations. Shaded areas denote 2-fold intervals around the predicted population mean. Smaller squares or circles represent individual datapoints, whereas larger symbols denote mean data. Error bars represent reported standard deviations. See Table 2 for simulation trial settings and Supplemental Tables 4 and 5 for additional demographic and bioanalytical details regarding the observed data.

4. Discussion

Knowledge of the extent to which drugs distribute to tissues is essential for exposure-response relationships when drug targets are located outside the vasculature. Measuring tissue concentrations is often not possible and predictive methods for the estimation of effect site concentrations such as PBPK are therefore of great utility. In the present study, the accuracy of PBPK for the prediction of plasma and tissue concentrations was evaluated. This was done by comparing observed clinical data from literature sources with PBPK model predictions for five beta-lactam antibiotics.

The observed plasma concentrations were well captured by the PBPK models, which gives some confirmation that inaccuracies in tissue predictions are not the result of mis-specified plasma predictions. Additionally, it serves as an external verification of the previously published models and a supplementary verification for the developed model for piperacillin. These verifications, however, are somewhat limited as only relatively healthy adult populations and mostly single-dose regimens were evaluated.

Predictions of total tissue concentrations in adipose, bone, and muscle tissue were less accurate than corresponding plasma predictions. This is not surprising given the inherent sampling and analytical challenges associated with quantifying drugs in tissue biopsy samples (Lin, 2006). A slight trend for underpredicted concentrations has also been discerned. As most studies did not correct for blood contamination (Supplemental Table 5), observed concentrations could have been artificially elevated due to blood containing microvasculature in the biopsy samples. Another major drawback of the observed total tissue concentrations was that the sampling points were generally more sparse than the plasma sample points and that the first sample was often taken some time after administration of the antibiotic, which makes assessments about the initial shape of the profile (distribution phase) difficult. This is intrinsic to the sample type due to it being unfeasible/unethical to take multiple tissue biopsy samples in the same patient or before adequate antibiotic levels are reached. Inaccuracies might also have been caused by the fact that PBPK models lack spatial resolution for adipose, muscle and bone tissue, both in location within the body and within the tissues. For example, while the differences in composition of cortical and cancellous bone are known to impact antibiotic penetration (Landersdorfer et al., 2009), no distinction between these bone segments are made in the model. Similarly, identical concentration-time profiles will be predicted for visceral and subcutaneous fat, while perfusion and composition of these adipose tissues differ (Virtanen et al., 2002; Lafontan, 2013). It has also been stated that the equations typically used to model perfusion-limited tissue distribution are not always correct, and that a distinction needs to be made between perfused and total volume (Berezhkovskiy, 2010; Thompson and Beard, 2011). The choice of an alternative Kp estimation method could also have altered model performance, as is evident by the large variability in Kp values originating from different methods (Supplemental Table 1). However, no attempt was made to identify the best Kp value for each drug/study, as changing a Kp value also impacts the estimated volume of distribution and plasma concentrations (Supplemental Figure 3). A fitting tool would be required which optimizes the Kp value in function of both tissue and plasma concentrations, but this is currently lacking in the PBPK software. To the best of our knowledge, the recent work of Garreau et al. is the only PBPK study which verified perfusion-limited tissue concentration profiles with observed data. They found that predictions of daptomycin bone and skin concentrations were within

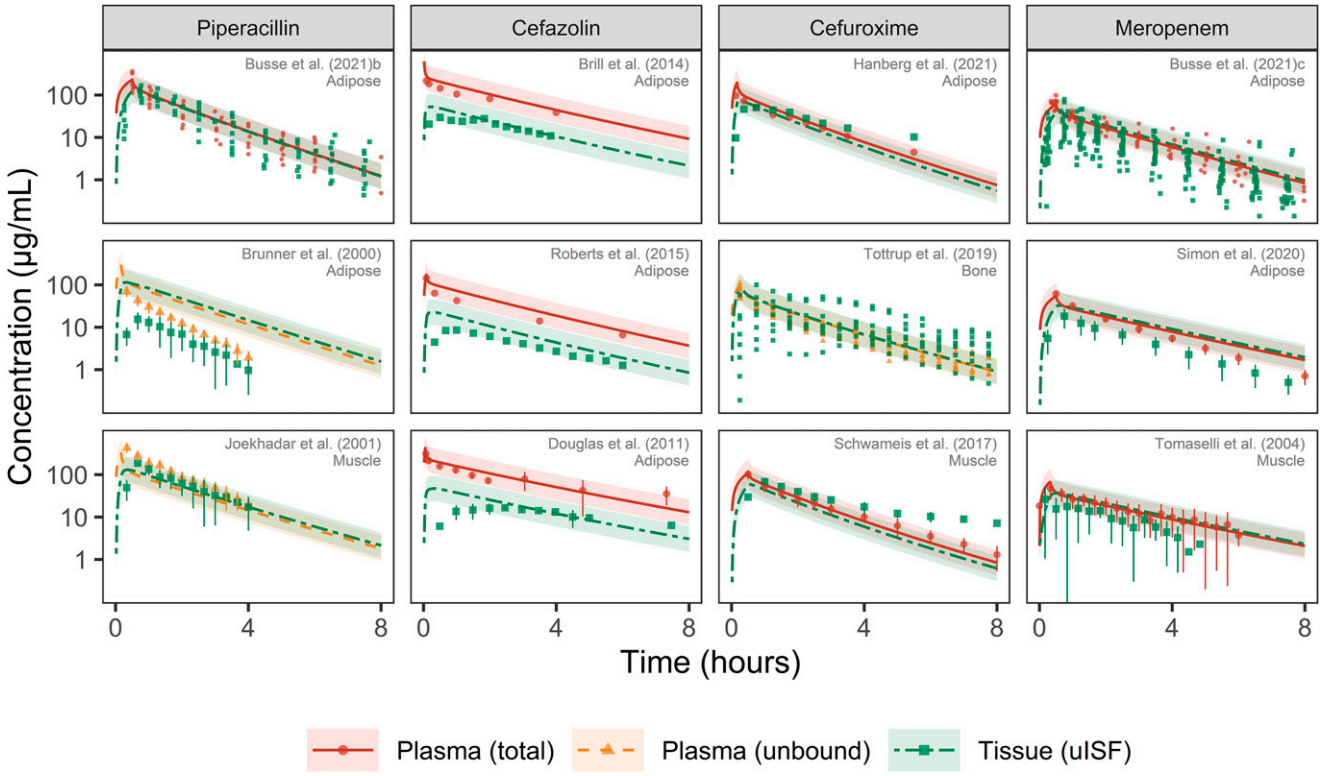

Fig. 2. PBPK-predicted (lines) and observed (squares, circles, and triangles) concentrations of four beta-lactam antibiotics in the interstitial fluid of perfusion-limited tissues and plasma. Unbound plasma concentrations (orange triangles) are shown when total plasma concentrations (red circles) were not reported. Tissue concentrations (green squares) are microdialysis-sampled uISF. Shaded areas denote 2-fold intervals around the predicted population mean. Smaller squares or circles represent individual datapoints, whereas larger symbols denote mean data. Error bars represent reported standard deviations. See Table 2 for simulation trial settings and Supplemental Tables 4 and 5 for additional demographic and bioanalytical details regarding the observed data.

2-fold of observed values (Garreau et al., 2022), which concurs with the results presented here.

In perfusion-limited PBPK models, concentrations in tissues are mostly represented as total concentrations, without a distinction between interstitial and intracellular concentrations. As uISF concentrations are the relevant (effect site) concentrations of beta-lactam antibiotics, the total concentrations were converted to uISF concentrations. Predictions of these uISF concentrations were generally less accurate than plasma and total tissue predictions, with a trend for overprediction. These overpredictions suggest that reaching an equilibrium between plasma and interstitial space is slower than expected or is not reached at all. Multiple included studies indeed indicated a longer time to maximum concentration in tissue than predicted by the PBPK models (Douglas et al., 2011; Brill et al., 2014; Roberts et al., 2015), which might suggest that the perfusion-limited well-stirred tank model does not adequately capture the distribution phase in tissues and permeability-limited models might need to be considered. It should be mentioned, however, that the length of microdialysis collection intervals (15–60 minutes, Supplemental Table 5) and differences in reported timepoints (midpoint versus endpoint of interval) makes a precise estimation of the observed time to maximum concentration difficult. As for the extent of distribution at equilibrium, the free drug hypothesis (i.e., the model assumption) implies that the ratio of the AUC of uISF to the AUC of unbound plasma approaches unity. This was not the case in multiple studies, with ratios

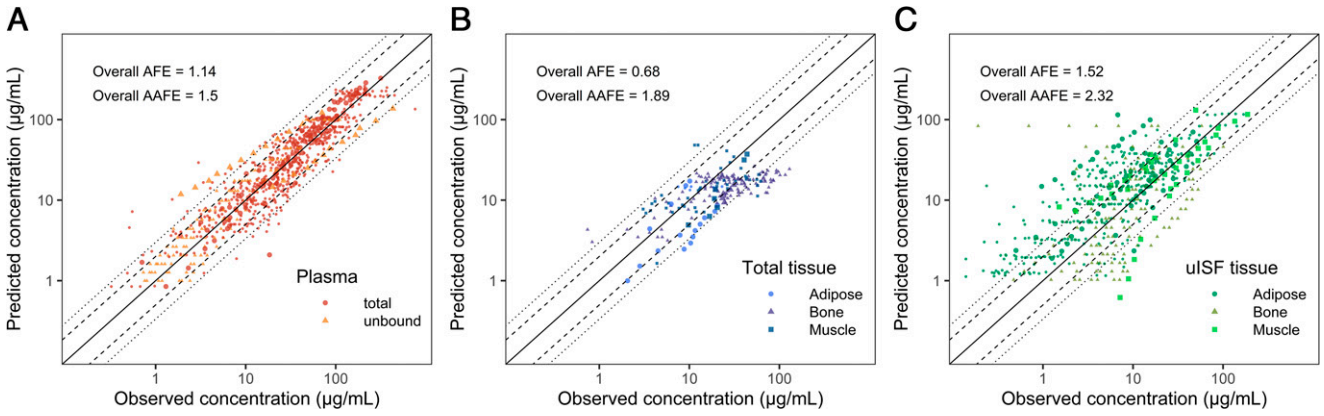

Fig. 3. Predicted versus observed concentrations of the five beta-lactams in plasma (A), total tissue biopsy homogenates (B) and uISF probed by microdialysis (C). Dashed and dotted lines denote 2- and 3-fold deviations from the line of unity, respectively. Smaller squares or circles represent individual datapoints whereas larger symbols denote mean data. The overall AFE and overall AAFE are averages of the AFE and AAFE of the specific studies.

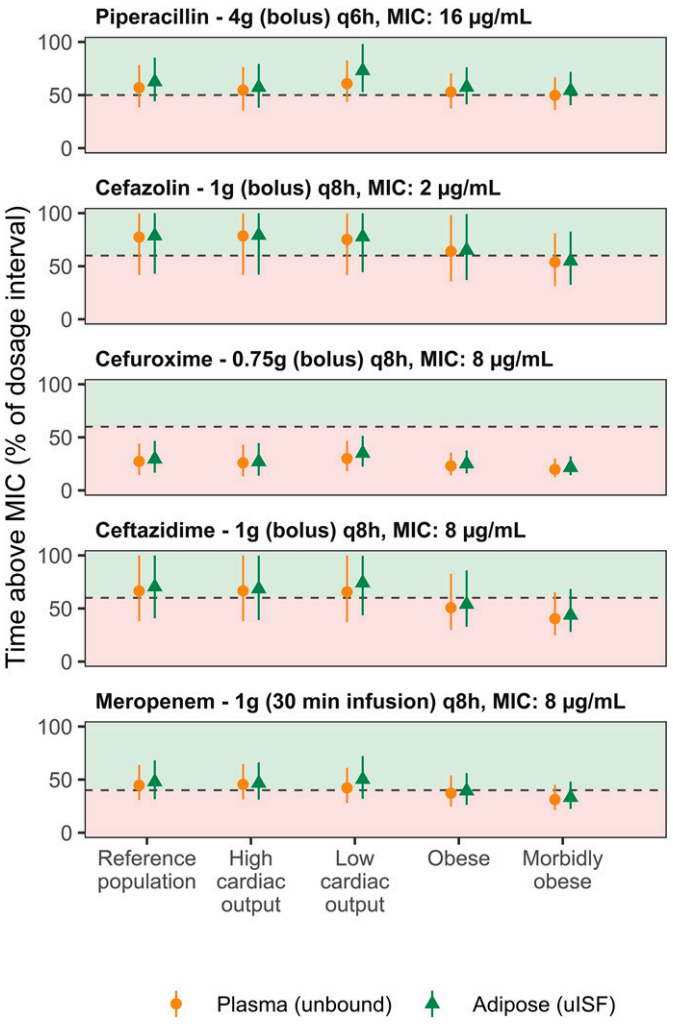

Fig. 4. Target attainment using standard dosages recommended by the European Committee on Antimicrobial Susceptibility Testing in five different virtual populations using different PBPK-predicted concentrations as input. The mean time the unbound plasma concentration (orange circles) and adipose uISF concentration (green triangles) exceed the non-species-specific resistant MIC is given as a percentage of the dosage interval, together with 5–95% percentiles (lines). The dashed lines represent conventional antibiotic-specific goals for target attainment. See Supplemental Fig. 4 and Supplemental Table 7 for the simulated profiles and population characteristics, respectively.

ranging between 0.3 (Busse et al., 2021c) and 1.8 (Schwameis et al., 2017). The limited dataset and large variability of uISF concentrations between and within studies does not allow for any statement to be made on whether this can be seen as evidence against the free drug hypothesis. More specifically, the between-subject variability in observed uISF concentrations was considerably larger than the 2-fold criteria in multiple studies (Tøttrup et al., 2019; Busse et al., 2021b; Busse et al., 2021c), which implies that even a perfectly specified mean prediction would have been associated with a larger AFE than tolerable. This can be explained by the fact that microdialysis procedures are known to be associated with a high degree of variability due to inter-individual and inter-catheter variability in relative recovery (Busse et al., 2021a). Consequently, the applied 2-fold criteria might be too stringent for uISF tissue predictions. As an alternative for fixed x-fold acceptance limits, alternative acceptance criteria based on the sample size and variation of the observed parameter have been proposed (Abduljalil et al., 2014). However, this method could not be consistently applied in this work due to missing variation measurements for observed concentrations.

PK/PD simulations show that using uISF instead of unbound plasma concentration did not result in significant changes to target attainment. For the investigated drugs and regimens the distribution phase barely influenced the target attainment rate, as the time it takes for the tissue concentrations to exceed the MIC was very limited relative to the dosing interval. Put differently, PBPK simulations showed only minor time delays (hysteresis) between plasma concentration and response (uISF adipose concentration). The time above MIC is even somewhat longer for uISF concentrations because in distribution equilibrium they slightly exceed the unbound plasma concentrations. This seemingly unexpected finding can be explained by the equilibration delay between arterial and venous concentrations, which stems from the time blood takes to circulate between these two pools. As the tissue concentration is assumed to be in equilibrium with the arterial concentration (well-stirred tank model), it follows that it will be different from the sampled venous plasma concentration (Musther et al., 2015). Either way, as the simulations do not show pronounced distributional hysteresis for the evaluated tissues and antibiotics, the added value of effect-site concentrations appears limited in this case.

The accuracy assessment of PBPK predicted tissue concentrations was focused on relatively healthy adult subjects and tissues. This approach was chosen as current PBPK models of perfusion-limited tissues are limited in their functionality to distinguish between healthy and sick tissue. For example, while there are reports that septic shock impacts tissue penetration (Joukhadar et al., 2001), important tissue alterations associated with sepsis such as capillary leakage and microcirculation abnormalities cannot be modeled in current PBPK models (Ibarra et al., 2020; Sanz Codina and Zeitlinger, 2022). Tissue perfusion, expressed as the tissue blood flow over volume ratio, can be changed however and the effect of varying this parameter on target attainment was evaluated. Differences in target attainment between unbound plasma and uISF became larger when cardiac output was decreased, which is in line with the previous statement on delay between venous and arterial concentrations. The simulated obese populations showed a lower target attainment than the reference population in unbound plasma, probably due to elevated renal function and bodyweight in these patients. However, differences in target attainment between uISF and unbound plasma were similar as in the reference population. This is in contrast with some reports which note less tissue distribution in obese patients relative to healthy volunteers (Toma et al., 2011; Brill et al., 2014), while in other studies, no difference in relative distribution could be discerned (Busse et al., 2021b; Busse et al., 2021c). Overall, the PK/PD simulations of the investigated beta-lactams show a limited impact of changing physiology on simulated uISF penetration.

In conclusion, PBPK-predicted tissue concentrations were found to be less accurate than concurrent plasma concentrations but generally were within 3-fold of observed data. These results imply that tissue predictions originating from PBPK models only verified with plasma data should be interpreted with caution.

Authorship Contributions

Participated in research design: De Sutter, De Cock, Gasthuys, Vermeulen.

Conducted experiments: De Sutter.

Performed data analysis: De Sutter.

Wrote or contributed to the writing of the manuscript: De Sutter, De Cock, Johnson, Musther, Gasthuys, Vermeulen.

References

Abdul-Aziz MH, Alffenaar C, Bassetti M, Bracht H, Dimopoulos G, Marriott D, Neely MN, Paiva J-A, Pea F, Sjovall F et al. (2020) Antimicrobial therapeutic drug monitoring in critically ill adult patients: a Position Paper. *Intensive Care Med* **46**:1127–1153.

Abduljalil K, Cain T, Humphries H, and Rostami-Hodjegan A (2014) Deciding on success criteria for predictability of pharmacokinetic parameters from in vitro studies: an analysis based on in vivo observations. *Drug Metab Dispos* **42**:1478–1484.

Abduljalil K, Ning J, Pansari A, Pan X, and Jamei M (2022) Prediction of Maternal and Fetoplacental Concentrations of Cefazolin, Cefuroxime, and Amoxicillin during Pregnancy Using Bottom-Up Physiologically Based Pharmacokinetic Models. *Drug Metab Dispos* **50**:386–400.

Alhadab AA and Brundage RC (2020) Physiologically-Based Pharmacokinetic Model of Sertraline in Human to Predict Clinical Relevance of Concentrations at Target Tissues. *Clin Pharmacol Ther* **108**:136–144.

Benet LZ, Broccatelli F, and Oprea TI (2011) BDDCS applied to over 900 drugs. *AAPS J* **13**: 519–547.

Berezhkovskiy LM (2010) A valid equation for the well-stirred perfusion limited physiologically based pharmacokinetic model that consistently accounts for the blood-tissue drug distribution in the organ and the corresponding valid equation for the steady state volume of distribution. *J Pharm Sci* **99**:475–485 Elsevier.

Berezhkovskiy LM (2004) Volume of distribution at steady state for a linear pharmacokinetic system with peripheral elimination. *J Pharm Sci* **93**:1628–1640.

Brill MJE, Houwink API, Schmidt S, Van Dongen EPA, Hazebroek EJ, van Ramshorst B, Deneer VH, Mouton JW, and Knibbe CAJ (2014) Reduced subcutaneous tissue distribution of cefazolin in morbidly obese versus non-obese patients determined using clinical microdialysis. *J Antimicrob Chemother* **69**:715–723.

Brunner M, Pernerstorfer T, Mayer BX, Eichler HG, and Müller M (2000) Surgery and intensive care procedures affect the target site distribution of piperacillin. *Crit Care Med* **28**:1754–1759.

Bulitta JB, Kinzig M, Jakob V, Holzgrabe U, Sörgel F, and Holford NHG (2010) Nonlinear pharmacokinetics of piperacillin in healthy volunteers–implications for optimal dosage regimens. *Br J Clin Pharmacol* **70**:682–693.

Busse D, Simon P, Michelet R, Ehmann L, Mehner F, Dorn C, Kratzer A, Huisinga W, Wrigge H, Petroff D et al. (2021c) Quantification of microdialysis related variability in humans: Clinical trial design recommendations. *Eur J Pharm Sci* **157**:105607.

Busse D, Simon P, Petroff D, Dorn C, Schmitt L, Bindellini D, Kratzer A, Dietrich A, Zeitlinger M, Huisinga W et al. (2021a) Similar Piperacillin/Tazobactam Target Attainment in Obese versus Nonobese Patients despite Differences in Interstitial Tissue Fluid Pharmacokinetics. *Pharmaceutics* **13**:1380.

Busse D, Simon P, Schmitt L, Petroff D, Dorn C, Dietrich A, Zeitlinger M, Huisinga W, Michelet R, Wrigge H et al. (2021b) Comparative Plasma and Interstitial Tissue Fluid Pharmacokinetics of Meropenem Demonstrate the Need for Increasing Dose and Infusion Duration in Obese and Non-obese Patients. *Clin Pharmacokinet* **61**:655–672 10.1007/s40262-021-01070-6.

Cristea S, Krekels EHJ, Allegaert K, De Paepe P, de Jaeger A, De Cock P, and Knibbe CAJ (2021) Estimation of Ontogeny Functions for Renal Transporters Using a Combined Population Pharmacokinetic and Physiology-Based Pharmacokinetic Approach: Application to OAT1,3. *AAPS J* **23**:65.

Douglas A, Udy AA, Wallis SC, Jarrett P, Stuart J, Lassig-Smith M, Deans R, Roberts MS, Taraporewalla K, Jenkins J et al. (2011) *Plasma and Tissue Pharmacokinetics of Cefazolin in Patients Undergoing Elective and Semielective Abdominal Aortic Aneurysm Open Repair Surgery. Antimicrobial Agents and Chemotherapy*, American Society for Microbiology.

Eichler H-G and Müller M (1998) Drug distribution. The forgotten relative in clinical pharmacokinetics. *Clin Pharmacokinet* **34**:95–99.

El-Khateeb E, Burkhill S, Murby S, Amirat H, Rostami-Hodjegan A, and Ahmad A (2021) Physiological-based pharmacokinetic modeling trends in pharmaceutical drug development over the last 20-years; in-depth analysis of applications, organizations, and platforms. *Biopharm Drug Dispos* **42**:107–117.

Fisher JW, Wu H, Cohen-Wolkowiez M, Watt K, Wang J, Burckart GJ, Troutman JA, and Yang X (2019) Predicting the pharmacokinetics of piperacillin and tazobactam in preterm and term neonates using physiologically based pharmacokinetic modeling. *Comput Toxicol* **12**:100104.

Fratoni AJ, Nicolau DP, and Kuti JL (2021) A guide to therapeutic drug monitoring of β-lactam antibiotics. *Pharmacotherapy* **41**:220–233.

Gaohua L, Neuhoff S, Johnson TN, Rostami-Hodjegan A, and Jamei M (2016) Development of a permeability-limited model of the human brain and cerebrospinal fluid (CSF) to integrate known physiological and biological knowledge: Estimating time varying CSF drug concentrations and their variability using in vitro data. *Drug Metab Pharmacokinet* **31**:224–233.

Garreau R, Montange D, Grillon A, Jehl F, Ferry T, Bourguignon L, and Goutelle S (2022) Daptomycin Physiology-Based Pharmacokinetic Modeling to Predict Drug Exposure and Pharmacodynamics in Skin and Bone Tissues. *Clin Pharmacokinet* **61**:1443–1456 DOI: 10.1007/s40262-022-01168-5.

Gergs U, Becker L, Okoniewski R, Weiss M, Delank K-S, and Neumann J (2020) Population pharmacokinetics of cefuroxime and uptake into hip and spine bone of patients undergoing orthopaedic surgery. *J Pharm Pharmacol* **72**:364–370.

Ghobadi C, Johnson TN, Aarabi M, Almond LM, Allabi AC, Rowland-Yeo K, Jamei M, and Rostami-Hodjegan A (2011) Application of a systems approach to the bottom-up assessment of pharmacokinetics in obese patients: expected variations in clearance. *Clin Pharmacokinet* **50**:809–822.

Guo Y, Chu X, Parrott NJ, Brouwer KLR, Hsu V, Nagar S, Matsson P, Sharma P, Snoeys J, Sugiyama Y et al.; International Transporter Consortium (2018) Advancing Predictions of Tissue and Intracellular Drug Concentrations Using In Vitro, Imaging and Physiologically Based Pharmacokinetic Modeling Approaches. *Clin Pharmacol Ther* **104**:865–889.

Hanberg P, Bue M, Kabel J, Jørgensen AR, Jessen C, Søballe K, and Stilling M (2021) Effects of tourniquet inflation on peri- and postoperative cefuroxime concentrations in bone and tissue. *Acta Orthop* **92**:746–752.

Holt K, Nagar S, and Korzekwa K (2019) Methods to Predict Volume of Distribution. *Curr Pharmacol Rep* **5**:391–399.

Hsu V, de L T Vieira M, Zhao P, Zhang L, Zheng JH, Nordmark A, Berglund EG, Giacomini KM, and Huang SM (2014) Towards quantitation of the effects of renal impairment and probenecid inhibition on kidney uptake and efflux transporters, using physiologically based pharmacokinetic modelling and simulations. *Clin Pharmacokinet* **53**:283–293.

Huizinga WKJ, Hirshberg A, Thomson SR, Elson KI, Salisbury RT, and Brock-Utne JG (1989) Prophylactic parenteral cefuroxime: subcutaneous concentrations in laparotomy wounds. *J Hosp Infect* **13**:395–398.

Ibarra M, Vázquez M, and Fagiolino P (2020) Current PBPK Models: Are They Predicting Tissue Drug Concentration Correctly? *Drugs R D* **20**:295–299.

Incavo SJ, Ronchetti PJ, Choi JH, Wu H, Kinzig M, and Sörgel F (1994) Penetration of piperacillin-tazobactam into cancellous and cortical bone tissues. *Antimicrob Agents Chemother* **38**:905–907.

Jamei M, Bajot F, Neuhoff S, Barter Z, Yang J, Rostami-Hodjegan A, and Rowland-Yeo K (2014) A mechanistic framework for in vitro-in vivo extrapolation of liver membrane transporters: prediction of drug-drug interaction between rosuvastatin and cyclosporine. *Clin Pharmacokinet* **53**:73–87.

Jamei M, Marciniak S, Feng K, Barnett A, Tucker G, and Rostami-Hodjegan A (2009) The Simcyp population-based ADME simulator. *Expert Opin Drug Metab Toxicol* **5**:211–223.

Jones H and Rowland-Yeo K (2013) Basic concepts in physiologically based pharmacokinetic modeling in drug discovery and development. *CPT Pharmacometrics Syst Pharmacol* **2**:e63.

Joukhadar C, Frossard M, Mayer BX, Brunner M, Klein N, Siostrzonek P, Eichler HG, and Müller M (2001) Impaired target site penetration of β-lactams may account for therapeutic failure in patients with septic shock. *Crit Care Med* **29**:385–391.

Kaukonen J-P, Tuomainen P, Mäkijärvi J, Mokka R, and Männistö PT (1995) Intravenous cefuroxime prophylaxis. Tissue levels after one 3-gram dose in 40 cases of hip fracture. *Acta Orthop Scand* **66**:14–16.

Kinzig M, Sörgel F, Brismar B, and Nord CE (1992) Pharmacokinetics and tissue penetration of tazobactam and piperacillin in patients undergoing colorectal surgery. *Antimicrob Agents Chemother* **36**:1997–2004.

Lafontan M (2013) Differences Between Subcutaneous and Visceral Adipose Tissues, in *Physiology and Physiopathology of Adipose Tissue* (Bastard J-P and Fève B, eds) pp 329–349, Springer, Paris.

Landersdorfer CB, Bulitta JB, Kinzig M, Holzgrabe U, and Sörgel F (2009) Penetration of antibacterials into bone: pharmacokinetic, pharmacodynamic and bioanalytical considerations. *Clin Pharmacokinet* **48**:89–124.

Lin JH (2006) Tissue distribution and pharmacodynamics: a complicated relationship. *Curr Drug Metab* **7**:39–65.

Loebis LH (1985) Tissue levels in patients after intravenous administration of ceftazidime. *J Antimicrob Chemother* **16**:757–761.

Mariappan TT, Mandlekar S, and Marathe P (2013) Insight into tissue unbound concentration: utility in drug discovery and development. *Curr Drug Metab* **14**:324–340.

Masich AM, Heavner MS, Gonzales JP, and Claeys KC (2018) Pharmacokinetic/Pharmacodynamic Considerations of Beta-Lactam Antibiotics in Adult Critically Ill Patients. *Curr Infect Dis Rep* **20**:9.

Mouton JW, Theuretzbacher U, Craig WA, Tulkens PM, Derendorf H, and Cars O (2008) Tissue concentrations: do we ever learn? *J Antimicrob Chemother* **61**:235–237.

Musther H, Gill KL, Chetty M, Rostami-Hodjegan A, Rowland M, and Jamei M (2015) Are Physiologically Based Pharmacokinetic Models Reporting the Right C(max)? Central Venous Versus Peripheral Sampling Site. *AAPS J* **17**:1268–1279.

Newsom SW, Palsingh J, Wells FC, and Kelly HC (1995) Penetration of meropenem into heart valve tissue. *J Antimicrob Chemother* **36** (Suppl A):57–62.

Ohge H, Takesue Y, Yokoyama T, Murakami Y, Hiyama E, Yokoyama Y, Kanehiro T, Itaha H, and Matsuura Y (1999) An additional dose of cefazolin for intraoperative prophylaxis. *Surg Today* **29**:1233–1236.

Plock N and Kloft C (2005) Microdialysis–theoretical background and recent implementation in applied life-sciences. *Eur J Pharm Sci* **25**:1–24.

Poulin P and Theil F-P (2002) Prediction of pharmacokinetics prior to in vivo studies. 1. Mechanism-based prediction of volume of distribution. *J Pharm Sci* **91**:129–156.

Roberts JA, Udy AA, Jarrett P, Wallis SC, Hope WW, Sharma R, Kirkpatrick CMJ, Kruger PS, Roberts MS, and Lipman J (2015) Plasma and target-site subcutaneous tissue population pharmacokinetics and dosing simulations of cefazolin in post-trauma critically ill patients. *J Antimicrob Chemother* **70**:1495–1502.

Rodgers T and Rowland M (2007) Mechanistic approaches to volume of distribution predictions: understanding the processes. *Pharm Res* **24**:918–933.

Rohatgi A (2021) Webplotdigitizer: Version 4.5.

Rowland M and Tozer TN (2011) Membranes and Distribution, in *Clinical Pharmacokinetics and Pharmacodynamics. Concepts and Applications,* pp 73–110, Lippincott Williams & Wilkins.

Russo Jr J, Thompson MI, Russo ME, Saxon BA, Matsen JM, Moody FG, and Rikkers LF (1982) Piperacillin distribution into bile, gallbladder wall, abdominal skeletal muscle, and adipose tissue in surgical patients. *Antimicrob Agents Chemother* **22**:488–492.

Sano T, Sakurai M, Dohi S, Oyama A, Murota K, Sugiyama H, Miura Y, Kusuoka K, and Kurata K (1993) [Investigation of meropenem levels in the human bone marrow blood, bone, joint fluid and joint tissues]. *Jpn J Antibiot* **46**:159–163.

Sanz Codina M and Zeitlinger M (2022) Biomarkers Predicting Tissue Pharmacokinetics of Antimicrobials in Sepsis: A Review. *Clin Pharmacokinet* **61**:593–617.

Schmitt W (2008) General approach for the calculation of tissue to plasma partition coefficients. *Toxicol In Vitro* **22**:457–467.

Schwameis R, Syré S, Marhofer D, Appelt A, Burau D, Sarahrudi K, Kloft C, and Zeitlinger M (2017) *Pharmacokinetics of Cefuroxime in Synovial Fluid. Antimicrobial Agents and Chemotherapy*, American Society for Microbiology, 10.1128/AAC.00992-17.

Simon P, Petroff D, Busse D, Heyne J, Girrbach F, Dietrich A, Kratzer A, Zeitlinger M, Kloft C, Kees F et al. (2020) Meropenem Plasma and Interstitial Soft Tissue Concentrations in Obese and Nonobese Patients-A Controlled Clinical Trial. *Antibiotics (Basel)* **9**:E931.

Sinagowitz E, Pelz K, Burgert A, and Kaczkowski W (1976) Concentrations of cefazolin in human skeletal muscle. *Infection* **4**:192–195.

Sörgel F and Kinzig M (1993) The chemistry, pharmacokinetics and tissue distribution of piperacillin/tazobactam. *J Antimicrob Chemother* **31** (Suppl A):39–60.

The European Committee on Antimicrobial Susceptibility Testing (2022) *Breakpoint tables for interpretation of MICs and zone diameters*.

Thompson MD and Beard DA (2011) Development of appropriate equations for physiologically based pharmacokinetic modeling of permeability-limited and flow-limited transport. *J Pharmacokinet Pharmacodyn* **38**:405–421.

Toma O, Suntrup P, Stefanescu A, London A, Mutch M, and Kharasch E (2011) Pharmacokinetics and tissue penetration of cefoxitin in obesity: implications for risk of surgical site infection. *Anesth Analg* **113**:730–737.

Tomaselli F, Maier A, Matzi V, Smolle-Jüttner FM, and Dittrich P (2004) Penetration of meropenem into pneumonic human lung tissue as measured by in vivo microdialysis. *Antimicrob Agents Chemother* **48**:2228–2232.

Tøttrup M, Søballe K, Bibby BM, Hardlei TF, Hansen P, Fuursted K, Birke-Sørensen H, and Bue M (2019) Bone, subcutaneous tissue and plasma pharmacokinetics of cefuroxime in total knee replacement patients - a randomized controlled trial comparing continuous and short-term infusion. *APMIS* **127**:779–788.

Utsey K, Gastonguay MS, Russell S, Freling R, Riggs MM, and Elmokadem A (2020) Quantification of the Impact of Partition Coefficient Prediction Methods on Physiologically Based Pharmacokinetic Model Output Using a Standardized Tissue Composition. *Drug Metab Dispos* **48**:903–916.

Virtanen KA, Lönnroth P, Parkkola R, Peltoniemi P, Asola M, Viljanen T, Tolvanen T, Knuuti J, Rönnemaa T, Huupponen R et al. (2002) Glucose uptake and perfusion in subcutaneous and visceral adipose tissue during insulin stimulation in nonobese and obese humans. *J Clin Endocrinol Metab* **87**:3902–3910.

Wen S, Wang C, Duan Y, Huo X, Meng Q, Liu Z, Yang S, Zhu Y, Sun H, Ma X et al. (2018) OAT1 and OAT3 also mediate the drug-drug interaction between piperacillin and tazobactam. *Int J Pharm* **537**:172–182.

Wittmann DH, Schassan HH, Kohler F, and Seibert W (1981) Pharmacokinetic studies of ceftazidime in serum, bone, bile, tissue fluid and peritoneal fluid. *J Antimicrob Chemother* **8** (Suppl B):293–297.

Yamada K, Matsumoto K, Tokimura F, Okazaki H, and Tanaka S (2011) Are bone and serum cefazolin concentrations adequate for antimicrobial prophylaxis? *Clin Orthop Relat Res* **469**:3486–3494.

Zhou W, Johnson TN, Xu H, Cheung S, Bui KH, Li J, Al-Huniti N, and Zhou D (2016) Predictive Performance of Physiologically Based Pharmacokinetic and Population Pharmacokinetic Modeling of Renally Cleared Drugs in Children. *CPT Pharmacometrics Syst Pharmacol* **5**:475–483.

Zhu L, Yang J, Zhang Y, Wang Y, Zhang J, Zhao Y, and Dong W (2015) Prediction of Pharmacokinetics and Penetration of Moxifloxacin in Human with Intra-Abdominal Infection Based on Extrapolated PBPK Model. *Korean J Physiol Pharmacol* **19**:99–104.

Zhu L, Zhang Y, Yang J, Wang Y, Zhang J, Zhao Y, and Dong W (2016) Prediction of the pharmacokinetics and tissue distribution of levofloxacin in humans based on an extrapolated PBPK model. *Eur J Drug Metab Pharmacokinet* **41**:395–402.

Zhu S, Zhang J, Lv Z, Zhu P, Oo C, Yu M, and Sy SKB (2022) Prediction of Tissue Exposures of Meropenem, Colistin, and Sulbactam in Pediatrics Using Physiologically Based Pharmacokinetic Modeling. *Clin Pharmacokinet* **61**:1427–1441.

Address correspondence to: Pieter-Jan De Sutter, Laboratory of Medical Biochemistry and Clinical Analysis, Ghent University, Campus Heymans, Ottergemsesteenweg 460, 9000 Gent, Belgium. E-mail: pieterjan.desutter@ugent.be